Catalytic Mechanism and Product Specificity of Rubisco Large Subunit Methyltransferase: QM/MM and MD Investigations†

Xiaodong Zhang and Thomas C. Bruice*

Department of Chemistry and Biochemistry, University of California at Santa Barbara, Santa Barbara, California 93106

Received January 19, 2007; Revised Manuscript Received March 7, 2007

ABSTRACT: Molecular dynamics (MD) simulations and hybrid quantum mechanics/molecular mechanics (QM/MM) calculations have been carried out in an investigation of Rubisco large subunit methyltransferase (LSMT). It was found that the appearance of a water channel is required for the stepwise methylation by *S*-adenosylmethionine (AdoMet). The water channel appears in the presence of AdoMet (LSMT·Lys-NH_3^+·AdoMet), but is not present immediately after methyl transfer (LSMT·Lys-N(Me)H_2^+·AdoHcy). The water channel allows proton dissociation from both LSMT·AdoMet·Lys-NH_3^+ and LSMT·AdoMet·Lys-N(Me)H_2^+. The water channel does not appear for proton dissociation from LSMT·AdoMet·Lys-$N(Me)_2H^+$, and a third methyl transfer does not occur. By QM/MM, the calculated free energy barrier of the first methyl transfer reaction catalyzed by LSMT (Lys-NH_2 + AdoMet → Lys-N(Me)H_2^+ + AdoHcy) is $\Delta G^{\ddagger} = 22.8 \pm 3.3$ kcal/mol. This $\Delta G^{\ddagger}$ is in remarkable agreement with the value 23.0 kcal/mol calculated from the experimental rate constant (6.2×10^{-5} s^{-1}). The calculated $\Delta G^{\ddagger}$ of the second methyl transfer reaction (AdoMet + Lys-N(Me)H → AdoHcy + Lys-$N(Me)_2H^+$) at the QM/MM level is 20.5 ± 3.6 kcal/mol, which is in agreement with the value 22.0 kcal/mol calculated from the experimental rate constant (2.5×10^{-4} s^{-1}). The third methyl transfer (Lys-$N(Me)_2$ + AdoMet → Lys-$N(Me)_3^+$ + AdoHcy) is associated with an allowed $\Delta G^{\ddagger}$ of 25.9 ± 3.2 kcal/mol. However, this reaction does not occur because a water channel does not form to allow the proton dissociation of Lys-$N(Me)_2H^+$. Future studies will determine whether the product specificity of lysine (mono, di, and tri) methyltransferases is determined by the formation of water channels.

S-adenosylmethionine (AdoMet) is the common methyl donor in the methyl transfer enzymes: M.HhaI DNA methyltransferase (*1*, *2*), guanidinoacetate methyltransferase (*3*), and protein lysine methyltransferase. All but one (*4*, *5*) of the known protein lysine methyltrasnferases catalyze all or part of the reactions shown in Scheme 1, including histone methyltransferase SET7/9 (*6*−*10*), SET8 (also known as PR-SET7) (*11*, *12*), *Neurospora* DIM-5 (*13*), histone lysine methyltransferase Clr4 (*14*), viral histone lysine methyltransferase (vSET) (*15*, *16*), and Rubisco large subunit methyltransferase (LSMT[1]) (*17*−*21*), and have a SET domain (*22*, *23*). A SET domain, originally identified in three *Drosophila* genes involved in epigenetic processes, contains approximately 130 amino acid residues.

The protein lysine methyltransferase's regulatory function lies in the ability of the enzyme to carry out varying numbers of methyl transfers to lysine (product specificity). Cheng et al. (*24*) showed that a tyrosine/phenylalanine switch in the structure of the protein lysine methyltransferase affects product specificity in that one methyl transfer becomes a transfer of two methyl groups. Trievel et al. (*18*) suggested that the CH−O hydrogen bonding between the methyl group of the methylated lysine and the tyrosine residues of the protein dominates the product specificity of the methyltransferases. To date, only one theoretical study (*25*) concerning catalytic mechanism and product specificity has been published. Hu et al. (*25*) employed *ab initio* quantum mechanics/molecular mechanics (QM/MM) free energy and molecular dynamics (MD) to study the catalytic mechanism and product specificity of SET7/9 and concluded that the methyl transfer reaction was a typical S_N2 reaction and that product specificity of SET7/9 was determined by the formation of near-attack conformations for the dimethylation reaction.

Scheme 1

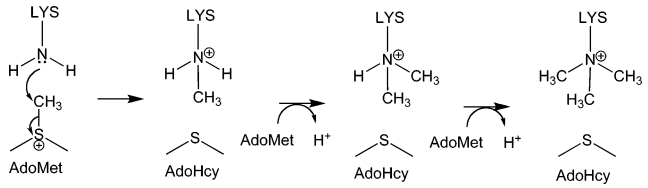

LSMT catalyzes the transfer of two methyl groups to the amino acid lysine (Scheme 1) (*21*). The second methyl transfer step is a little faster than the first methyl transfer step (*17*). Trievel et al. (*21*) have proposed that LSMT should be capable of multi-methylating a single lysine as a substrate. Rubisco LSMT is able to mono-, di-, and tri-methylate the Lys14 of a ∼30 amino acid peptide substrate (*19*, *20*). In

† This project was supported by NIH Grant 5R37DK9171-43.

* To whom correspondence should be addressed: Tel: 805-893-2044. Fax: 805-893-2229. E-mail: tcbruice@chem.ucsb.edu.

[1] Abbreviations: LSMT, rubisco large subunit methyltransferase; MD, molecular dynamics; QM/MM, quantum mechanics/molecular mechanics; SCCDFTB, selfconsistent charge density functional tight binding; CPR, conjugate peak refinement; TS, transition state.

10.1021/bi700119p CCC: $37.00
Published on Web 04/13/2007

Table 1: Average Density (in Atoms/Å^3) of the Water Molecules at the Positions of the Water Channel (Shown in Figures 2 and 8) during MD Simulations[a]

Complex	LSMT·AdoMet·Lys-NH_3^+ (Figure 2)									
positions	Wat143	A	B	C	D	E	F	G	H	
density	0.005	0.008	0.012	0.015	0.015	0.014	0.010	0.011	0.009	
Complex	LSMT·AdoMet·Lys-N(Me)H_2^+(Figure 8)									
positions	Wat6	A	Wat395	Wat559	B	C	D	E	F	G
density	0.006	0.008	0.010	0.014	0.018	0.016	0.018	0.018	0.016	0.011

[a] The solvent molecules are designated A−G, and the crystal molecules are designated Wat.

Table 2: Comparisons of the Reactant and Transition States for the First Methyl Transfer Step Catalyzed by LSMT and SET7/9

parameters	present study	Hu et al.(*22*)
reactant state		
Nϵ(Lys)···Cγ(AdoMet)	3.11 ± 0.11 Å	3.25 ± 0.06 Å
Nϵ(Lys)···Cγ(AdoMet)···Sδ(AdoMet)	162 ± 9°	153 ± 5°
transition state		
Nϵ(Lys)···Cγ(AdoMet)	2.28 ± 0.04 Å	2.30 ± 0.02 Å
Cγ(AdoMet)···Sδ(AdoMet)	2.26 ± 0.05 Å	2.32 ± 0.02 Å
Nϵ(Lys)···Cγ(AdoMet)···Sδ(AdoMet)	172 ± 2°	173 ± 1°

the present study, we employ hybrid QM/MM and MD simulations to investigate the reaction mechanism and product specificity of LSMT with a single lysine as a substrate. Our calculations establish that the formation of a water channel is required for lysine methylation by AdoMet.

MATERIALS AND METHODS

The initial structure of the LSMT·AdoMet·Lys complex was built from the X-ray structure of the LSMT enzyme with AdoHcy and the methylated Lys (MeLys) substrate (pdb entry: 1OZV (*17*)). The methyl group of enzyme-bound AdoMet was built on the basis of the LSMT·AdoHcy·MeLys structure. Rubisco LSMT is a trimer in the crystalline form (*26*) and a monomer in solution (*27*). The distance between any two active sites in the trimer is more than 95 Å. Thus, a single monomer was employed in this study.

A water (TIP3P (*28*)) sphere with a 25 Å radius was centered at the AdoMet cofactor. Hydrogen atoms were added to the crystal structure using the HBUILD module implemented in CHARMM (*29*) (version 31b1), and CHARMM31 force field parameters (*30*, *31*) were employed. A spherical boundary potential (*32*) for a 25 Å radius was used to prevent the water from "evaporating" from the surface. Each complex, including LSMT·AdoMet·Lys-NH_3^+, LSMT·AdoMet·Lys-NH_2, LSMT·AdoHcy·Lys-N(Me)H_2^+, LSMT·Lys-N(Me)H_2^+, LSMT·AdoMet·Lys-N(Me)H_2^+, LSMT·AdoMet·Lys-N(Me)H, LSMT·AdoMet·Lys-$N(Me)_2H^+$, and LSMT·AdoMet·Lys-$N(Me)_2$, was minimized by the Adopted Basis Newton−Rasphon (ABNR) method until the gradient was less than 0.01 kcal/(mol·Å) at the MM level. Stochastic boundary molecular dynamics (SBMD) (*33*) were carried out for 3.0 ns on each complex. An integration time-step of 1 fs was used, with all of the bonds involving hydrogen atoms constrained using SHAKE (*34*). Ten snapshots of each complex with neutral Lys were picked up from 500 to 3000 ps, with the interval being at least 200 ps. The presence of a water channel is established by determining the distances between the hydrogen and oxygen atoms of the continuous water molecules. A distance of 1.85 Å supports a water channel. The average densities of the water molecules in the water channel confirm the formation of a water channel. The pK_a of Lys-NH_3^+ in each of the 10 snapshots is estimated using the PBEQ (*35*, *36*) module implemented in CHARMM, with 4.0 as the dielectric constant of the protein at the MM level. For the pK_a calculations, the atomic radii are taken from ref 37 (*37*), and the partial charge of the neutral lysine residue is from ref 38 (*38*).

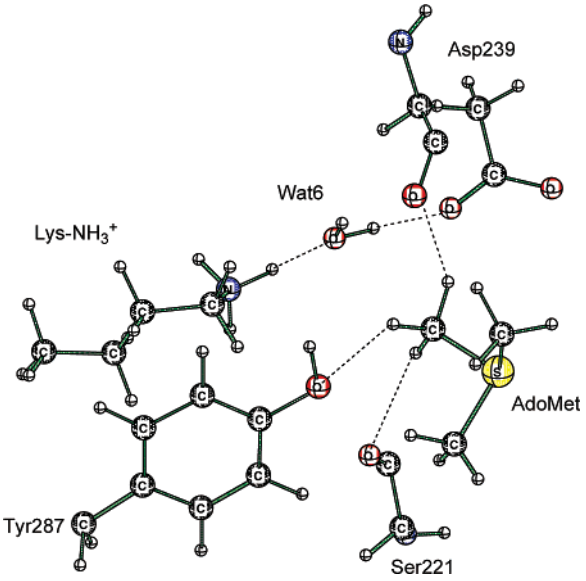

FIGURE 1: Structure at the active site of one snapshot from the molecular dynamics simulations on the LSMT·AdoMet·Lys-NH_3^+ complex.

Each of the 10 snapshots was minimized by QM/MM methods (QM = SCCDFTB (*39*, *40*), selfconsistent charge density functional tight binding) until the gradient was less than 0.01 kcal/(mol·Å), which led to an optimized structure of the reactant. In the QM/MM calculations, the QM region included the $-CH_2$-S^+(Me)-CH_2- part of the AdoMet cofactor and the side chain of the neutral lysine substrate (Lys-NH_2) (neutral monomethylated lysine or neutral dimethylated lysine). Link atoms were introduced to saturate the valence of the QM boundary atoms.

Adiabatic mapping calculations at the SCCDFTB/MM level were carried out using the two-dimensional (2D) potential energy surface (PES). The 2D reaction coordinates were the distances of N_ϵ(Lys)−C_γ(AdoMet) and C_γ(AdoMet)−S_δ(AdoMet). Calculations with the one-dimensional (1D) reaction coordinate ($s = d_{C\gamma(AdoMet)-S\delta(AdoMet)} - d_{N\epsilon(Lys)-C\gamma(AdoMet)}$) overestimate the reaction barrier. Thus, the 2D reaction coordinates have been used in the present studies. In the present study, the barrier with a 1D reaction coordinate was more than 3.0 kcal/mol greater than that with a 2D reaction coordinate. The transition states were obtained using con-

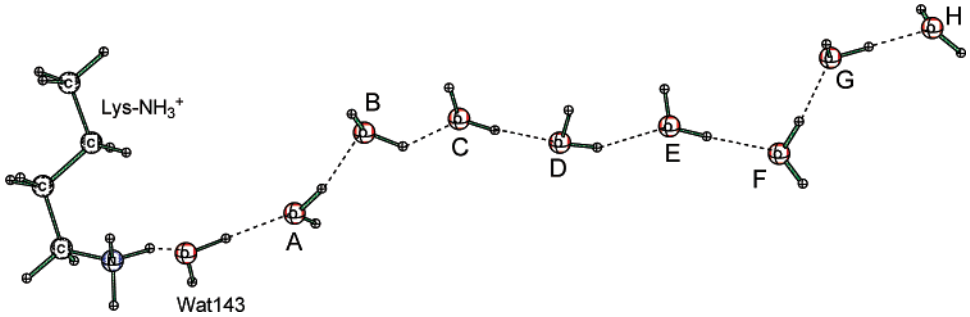

FIGURE 2: Water channel created upon the formation of the LSMT·AdoMet·Lys-NH_3^+ complex. The solvent water molecules are designated A−H, and H is on the surface of the water sphere of 25 Å radius. The crystal water molecule is denoted by Wat143.

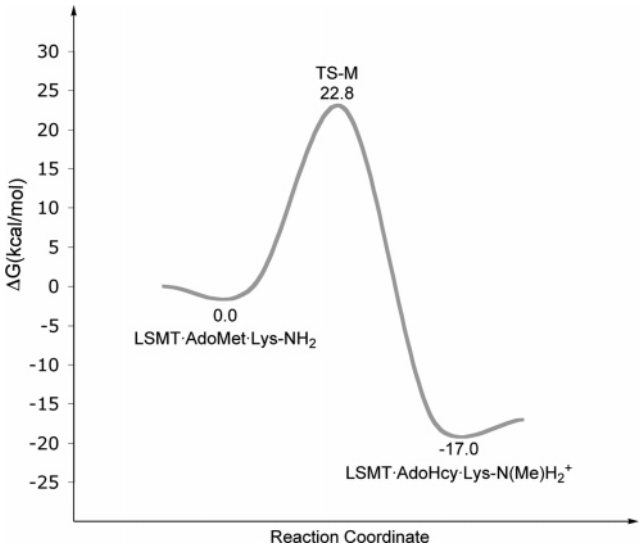

FIGURE 3: Schematic effective free energy surface for the first methyl transfer reaction Lys-NH_2 +AdoMet → Lys-N(Me)H_2^+ + AdoHcy catalyzed by LSMT.

jugate peak refinement (CPR) (*41*) implemented in the trajectory refinement and kinematics module of CHARMM, and normal-mode analysis provided only one imaginary frequency to characterize the transition state. To obtain more quantitative free energies of reactions, single-point computations at the MP2/6-31+G(d,p)//MM (Gamess-US version June 22, 2002) (*42*) level were carried out. The free energies were obtained using the equation $\Delta G = \Delta E + \Delta E_{Ther} + \Delta(ZPE) - T\Delta S$ (*43*). The potential energy (ΔE) was provided by QM/MM. The thermal energy (ΔE_{Ther}) could be expressed as $\Delta E_{Ther} = \Delta E_{Trans} + \Delta E_{Rot} + \Delta E_{Vib}$. The vibrational contributions ($\Delta(ZPE)$, ΔE_{vib}, and $-T\Delta S$) were determined with harmonic approximation at $T = 298$ K by normal-mode analysis. Because the thermal energies and entropies from the transition motion (E_{Trans}) and rotation motion (E_{Rot}) are linear with temperature according to their corresponding statistical equations, their contributions to the reaction barrier (or reaction energy) should be about zero for an enzymatic reaction at constant temperature.

The residues within 13 Å, which is the common nonbond distance in MD simulations, of AdoMet in all species (reactant, intermediate, transition state, and product) were included in the normal-mode analysis to provide $3N - 6$ frequencies, which were employed to calculate the zero-point energy, the thermal vibrational energy, and the entropy. (N is the number of atoms within the reduced regions; residues beyond that were fixed in the vibrational calculations.)

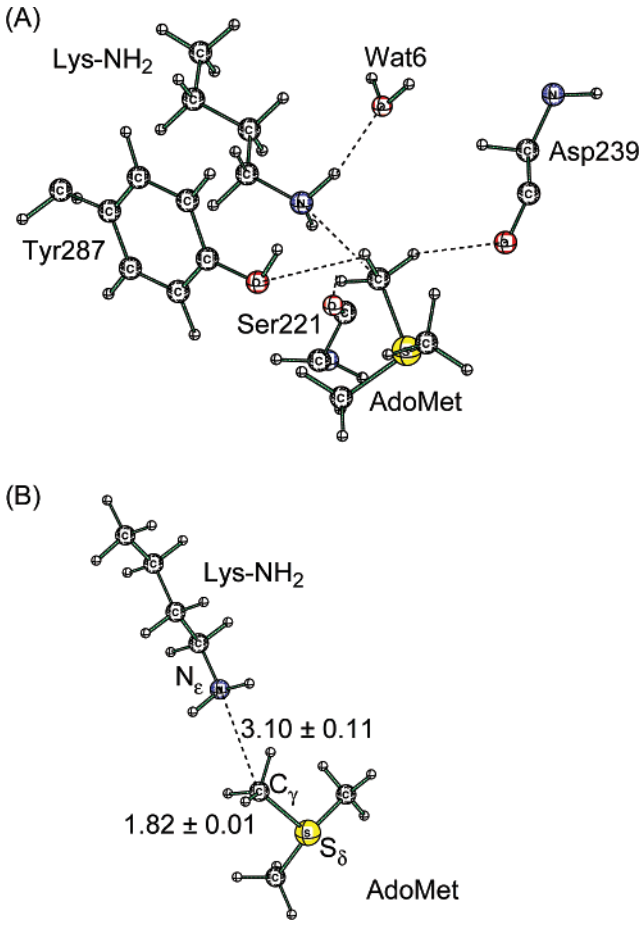

FIGURE 4: Structure of the ground state LSMT·AdoMet·Lys-NH_2 (A) and a close-up of the QM region (B) in the first methyl transfer reaction LSMT·AdoMet·Lys-NH_2 → LSMT·AdoHcy·Lys-N(Me)-H_2^+.

RESULTS AND DISCUSSION

First Methyl Transfer Reaction

Deprotonation of Lys-NH_3^+. Throughout the 3 ns MD simulations, a water channel is positioned to allow proton transfer from Lys-NH_3^+ to the water solvent (Figure 2). The hydrogen bonding between water molecules (<1.85 Å) and average densities (Table 1) of the channel water molecules confirm the presence of a water channel. Calculations (see the Materials and Methods section) establish that the average pK_a of enzyme-bound Lys-NH_3^+ is 8.0, and the deviation is ± 0.3. The small deviation of pK_a is dependent on the smaller fluctuation of the structures. Thus, neutral Lys-NH_2 is

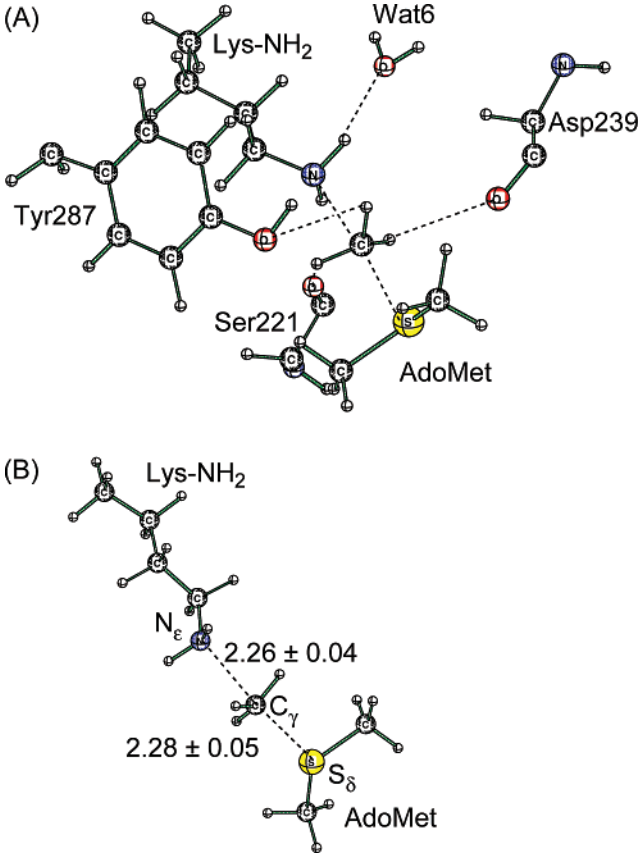

FIGURE 5: Structure of the transition state (TS−M) (A) and a close-up of the QM region (B) in the first methyl transfer reaction LSMT·AdoMet·Lys-NH_2 → LSMT·AdoHcy·Lys-N(Me)H_2^+.

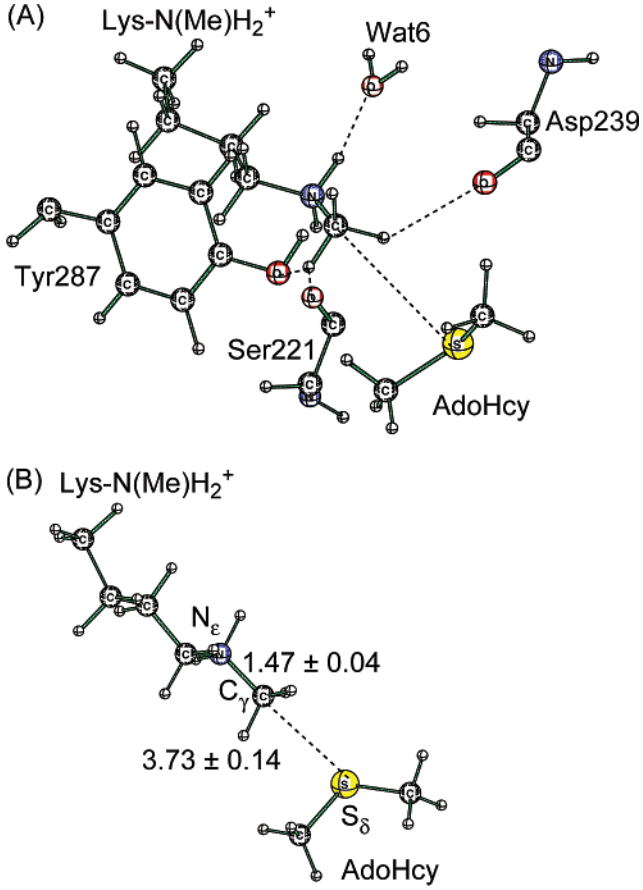

FIGURE 6: Structure of the immediate product LSMT·AdoHcy·Lys-N(Me)H_2^+ (A) and a close-up of the QM region (B) in the first methyl transfer reaction LSMT·AdoMet·Lys-NH_2 → LSMT·AdoHcy·Lys-N(Me)H_2^+.

available to be a substrate. Experiments show that LSMT is active at pH 8.0 or higher.

Lys-NH_3^+ is hydrogen bonded to the first water molecule of the water channel (Figure 2), in which one crystal water molecule (Wat143) is present. When a hydroxide ion is positioned at D (Figure 2), there is no barrier to proton transfer from Lys-NH_3^+ to HO^- at the QM/MM level (QM = both SCCDFTB and HF/6-31+G(d,p)). Because the concentration of HO^- at pH 8.0 is 10^{-6}, the activation energy barrier would be 8.4 kcal/mol. The barrier for deprotonation will be less than 8.4 kcal/mol when the pH is greater than 8.0.

An examination of the LSMT·AdoMet·Lys-NH_3^+ complex (Figure 1) establishes that hydrogen bonding between Asp239, Wat6, and Lys-NH_3^+. Asp239-CO_2^- cannot deprotonate Lys-NH_3^+ because the pK_a values of Asp239-CO_2H and Lys-NH_3^+ are ∼4.5 and ∼8.0, respectively. Therefore, Asp239-CO_2^- does not play a role in the first methyl transfer reaction.

Free Energy Profile for the First Methyl Transfer Reaction: LSMT·AdoMet·Lys-NH_2 → LSMT·AdoHcy·Lys-N(Me)H_2^+. The reaction coordinates for the first methyl transfer reaction are shown in Figure 3. The structures of the reactant, transition state, and product were determined by 2D SCCDFTB/MM. On the basis of these structures, single-point calculations at the MP2/6-31+G(d,p)//MM level were performed to obtain average potential energies. Average Δ(ZP*E*) and −TΔ*S* values were determined from harmonic normal-mode analysis.

The structure of the reactant is shown in Figure 4. In this structure, the substrate has been formed by the loss of a proton from Lys-NH_3^+. The S_δ(AdoMet)···C_γ(AdoMet)···N_ϵ(Lys-NH_2) (162 ± 9°) is almost linear, favoring an S_N2 methyl transfer reaction. In the structure of the ground state (Figure 4), the bond lengths of both N_ϵ(Lys)−C_γ(AdoMet) and C_γ(AdoMet)−S_δ(AdoMet) are 3.10 ± 0.11 and 1.82 ± 0.01 Å, respectively. The calculated average potential energy barrier for the first methyl transfer reaction is $\Delta E^\ddagger$ = 21.4 ± 3.2 kcal/mol. The structure of the transition state (TS−M) for the first methyl transfer reaction (Figure 5) was located by CPR (*41*) at the SCCDFTB/MM level. Normal-mode analysis characterizes the TS−M with only one imaginary frequency of 275 ± 88i cm^{-1}. In the TS−M (Figure 5), the bond lengths of N_ϵ(Lys)−C_γ(AdoMet) and C_γ(AdoMet)−S_δ(AdoMet) are 2.28 ± 0.05 and 2.26 ± 0.04 Å, respectively, and the N_ϵ(Lys)−C_γ(AdoMet)−S_δ(AdoMet) bond angle is 172 ± 2 °. Hu et al. (*25*) recently reported a transition state of the methyl transfer reaction catalyzed by the monomethyltransferase SET7/9. The nearly identical geometrical parameters (Table 2) suggest that the first methyl transfer reactions catalyzed by LSMT and SET7/9 have the same mechanism.

The average contributions of $\Delta(ZPE)^\ddagger$ = 0.39 ± 0.41 kcal/mol, $-T\Delta S^\ddagger$ = 1.34 ± 1.22 kcal/mol, and $\Delta E_{vib}^\ddagger$ = −0.33 ± 0.22 kcal/mol to the reaction barrier of the first methyl transfer reaction were provided by normal-mode analysis.

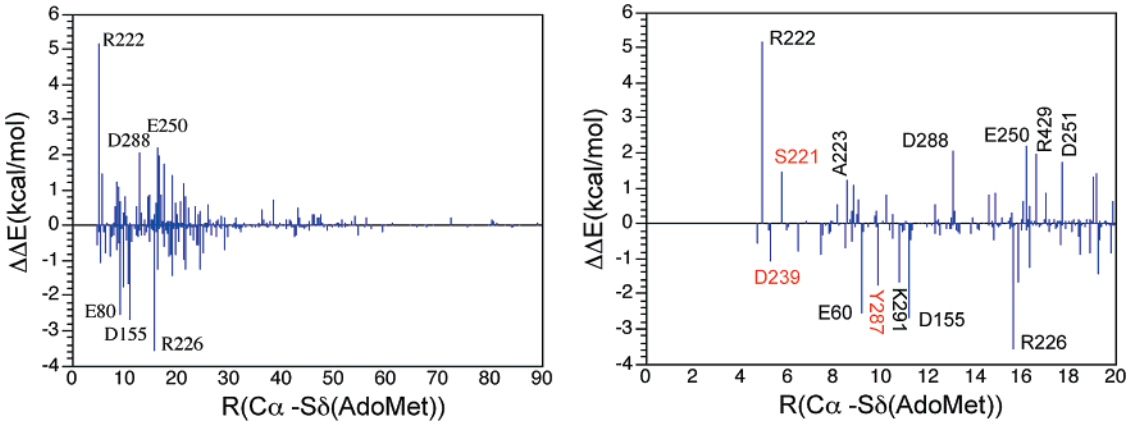

FIGURE 7: Results from perturbation analysis for the contribution from the protein residues to the activation barrier of LSMT·AdoMet·Lys-NH_2 → LSMT·AdoHcy·Lys-N(Me)H_2^+. The positive values indicate the favorable contributions that lower the barrier, and the negative values indicate the unfavorable contributions that increase the barrier.

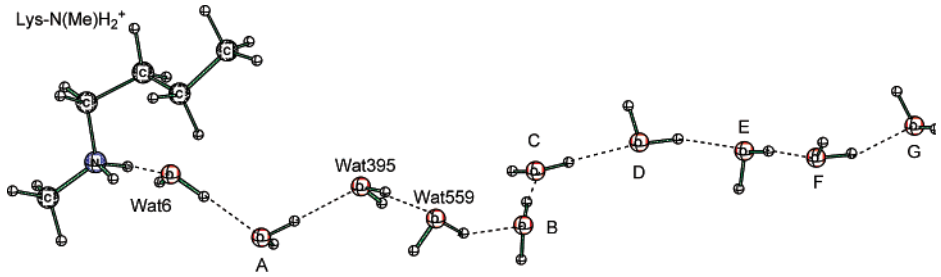

FIGURE 8: Water channel created upon the formation of the LSMT·AdoMet·Lys-N(Me)H_2^+ complex. Water molecules are designated A−G, and G is on the surface of the water sphere of 25 Å radius. The three crystal water molecules are denoted by Wat6, Wat395, and Wat559.

Table 3: Distances (in Å) and the Corresponding Difference of the Key Hydrogen Bonding at the Active Site of the Transition State and the Reactant for the First Methyl Transfer Reaction Catalyzed by LSMT

	reactant		TS		difference	
hydrogen bonds	average	deviation	average	deviation	average	deviation
HZ1(Lys)−O(S221)	3.88	0.87	3.80	0.56	−0.08	0.50
HZ2(Lys)−OH2(Wat6)	2.73	0.64	3.26	0.75	0.53	0.60
HT1(Lys)−OH(Y300)	2.75	0.68	2.72	0.68	−0.03	0.06
HT3(Lys)−O(Y287)	4.34	1.09	4.35	1.11	0.00	0.03
HGP1(AdoMet)−O(D239)	3.34	0.79	3.23	0.63	−0.10	0.36
HGP2(AdoMet)−OH(Y287)	3.83	0.54	3.71	0.56	−0.12	0.14
HGP3(AdoMet)−O(S221)	3.10	0.56	3.12	0.54	0.02	0.21
H3T(AdoMet)−O(Y300)	3.02	0.48	3.03	0.49	0.01	0.02
OT1(AdoMet)−HH21(R222)	2.36	0.65	2.33	0.66	−0.02	0.03

The average free energy barrier to the first methyl transfer reaction is $\Delta G^{\ddagger} = \Delta E^{\ddagger} + \Delta(ZPE)^{\ddagger} - T\Delta S^{\ddagger} + \Delta E_{vib}{}^{\ddagger} = 21.4 + 0.39 + 1.34 - 0.33 = 22.8$ kcal/mol (Figure 3), which is in excellent agreement with the free energy barrier (23.0 kcal/mol) calculated from the experimental rate constant (6.2×10^{-5} s^{-1}) (*17*). The deviation of $\Delta G^{\ddagger}$ is ±3.3 kcal/mol.

The first methyl transfer reaction is calculated to be exergonic overall: $\Delta G^{\circ} = \Delta E^{\circ} + \Delta(ZPE)^{\circ} - T\Delta S^{\circ} + \Delta E_{vib}{}^{\circ} = -22.1 + 3.9 + 1.7 - 0.6 = -17.0$ kcal/mol (Figure 3). The deviations in ΔG°, ΔE°, $\Delta(ZPE)^{\circ}$, $T\Delta S^{\circ}$, and $\Delta E_{vib}{}^{\circ}$ are ±6.1, ±6.7, ±0.6, ±1.4, and ±0.4 kcal/mol, respectively. The structure of the immediate product is shown in Figure 6. The N_{ϵ}(Lys)−C_{γ}(AdoMet)−S_{δ}(AdoMet) bond angle is 153 ± 6°, which is favorable for the initiation of the second methyl transfer reaction (LSMT·AdoMet·Lys-N(Me)H → LSMT·AdoHcy·Lys-N(Me)$_2$$H^+$).

Perturbation Analysis of the Contribution from Electrostatic Interactions. In going from the reactant to the transition state in the first methyl transfer reaction, the lengths of the key hydrogen bonds (Table 3) are not significantly changed (Figures 4−6). Thus, the contributions of van der Waals interactions to the free energy barrier from Ser221, Arg222, Asp239, Tyr287, and Tyr300 are small. The contribution of electrostatic effects to catalysis is defined as the difference ($\Delta\Delta E$) in the calculated activation energies for a residue with no charge and with its normal partial charge. The results at the level of QM/MM are shown in Figure 7. The perturbation analysis (*44*, *45*) of Figure 7 for the first methyl transfer reaction indicates that the dominant and favorable effects of Arg222 (5.16 ± 0.47 kcal/mol), Glu250 (2.21 ± 0.26 kcal/mol), Asp288 (2.03 ± 0.31 kcal/mol), Arg429 (1.98 ± 0.17 kcal/mol), Asp251 (1.71 ± 0.07 kcal/mol), Ser221 (1.43 ± 0.12 kcal/mol), and Glu255 (1.30 ± 0.17 kcal/mol) decrease the activation energy compared with that in solution or in the gas-phase model. These residues stabilize the transition state. The residues with unfavorable contributions to the reaction barrier, including Arg226 (−3.57 ± 0.53 kcal/mol), Asp155 (−2.70 ± 0.44 kcal/mol), Glu80 (−2.51 ± 0.58 kcal/

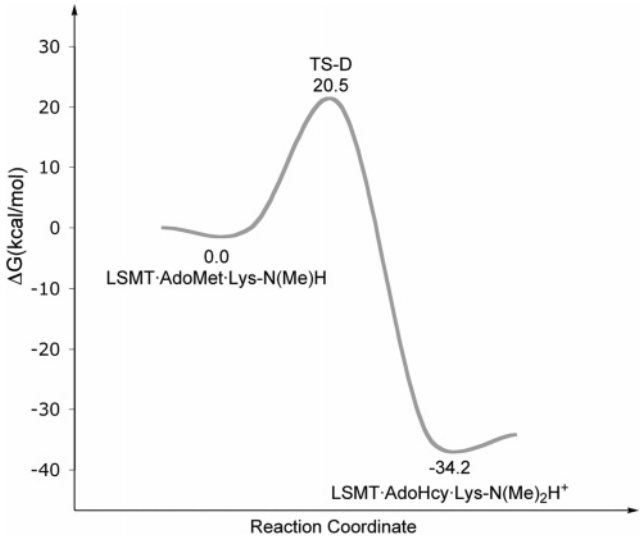

FIGURE 9: Schematic effective free energy surface for the second methyl transfer reaction Lys-N(Me)H + AdoMet → Lys-N(Me)$_2$H$^+$ + AdoHcy catalyzed by LSMT.

Scheme 2

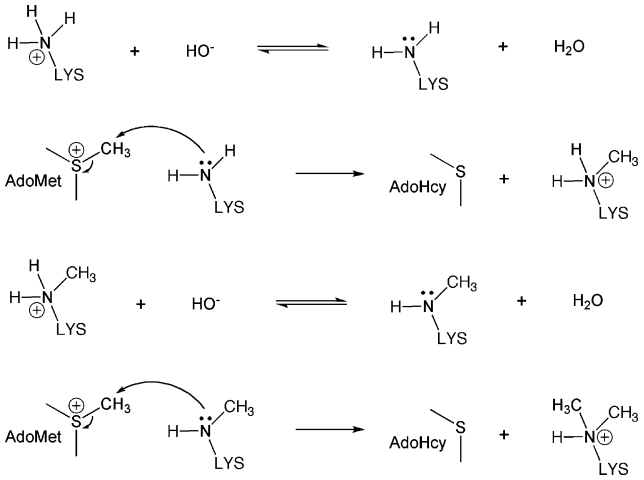

mol), Tyr287 (−1.75 ± 0.29 kcal/mol), Lys291 (−1.67 ± 0.22 kcal/mol), and Asp239 (−1.03 ± 0.30 kcal/mol), stabilize the ground state of E·S. Forces stabilizing ground and transition states are equal within a few kcal/mol.

Second Methyl Transfer Reaction

Lys-N(Me)H$_2^+$ Is a Stable Intermediate. The MD simulations on the immediate product of the first methyl transfer reaction (LSMT·AdoHcy·Lys-N(Me)H$_2^+$) failed to show a water channel that would allow proton dissociation from Lys-N(Me)H$_2^+$. When AdoHcy is released from the active site, the MD simulations on LSMT·Lys-N(Me)H$_2^+$ still do not indicate the formation of a water channel. These MD simulations support Lys-N(Me)H$_2^+$ as a stable intermediate. It is not until AdoMet replaces the spent AdoHcy at the active site that a water channel forms and is present during 3 ns of MD simulations. The densities (Table 1) of water molecules at the positions (Figure 8) confirm the formation of the water channel. The water channel involving Lys-N(Me)H$_2^+$ and water molecules is shown in Figure 8, in which there are three crystal water molecules (Wat6, Wat395, and Wat559). The lengths of the hydrogen bonds are all less than 1.85 Å. Thus, it is the AdoMet cofactor that induces the formation

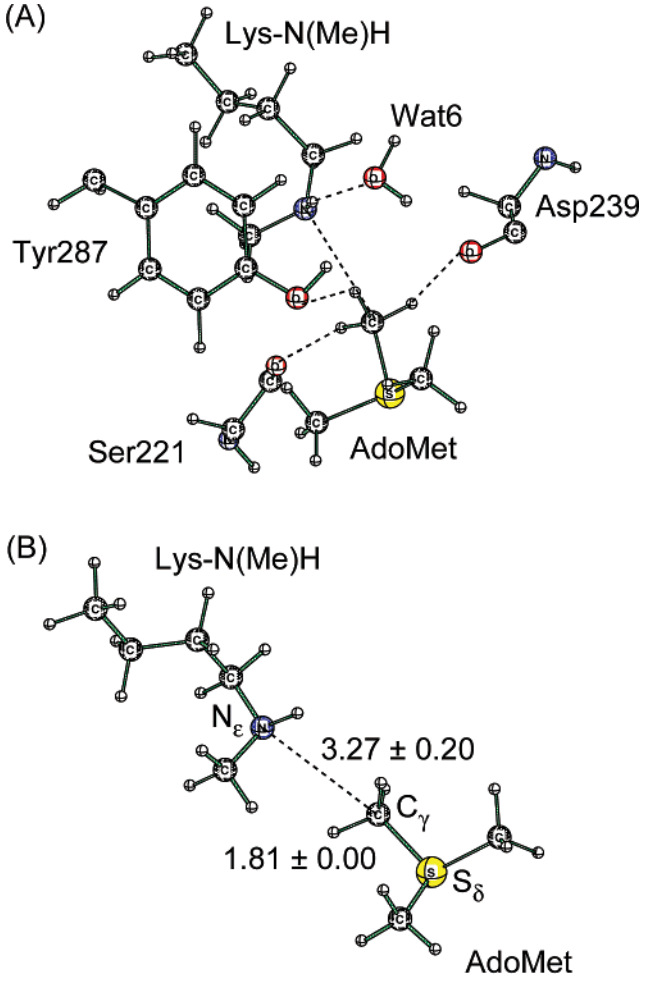

FIGURE 10: Structure of the ground state LSMT·AdoMet·Lys-N(Me)H (A) and a close-up of the QM region (B) in the second methyl transfer reaction LSMT·AdoMet·Lys-N(Me)H → LSMT·AdoHcy·Lys-N(Me)$_2$H$^+$.

of the water channel that causes deprotonation of Lys-N(Me)-H$_2^+$ in order to create the substrate for the second methyl transfer reaction. These MD simulations and QM/MM computations support the reaction sequence in Scheme 2.

Free Energy Profile for the Second Methyl Transfer Reaction: LSMT·AdoMet·Lys-N(Me)H → LSMT·AdoHcy·Lys-N(Me)$_2$H$^+$. The procedure used to obtain the free energy profile for the first methyl transfer reaction was also used for the second methyl transfer reaction (Figure 9). The average bond lengths of N_ϵ(MeLys)−C_γ(AdoMet) and C_γ-(AdoMet)−S_δ(AdoMet) in the reactant for the second methyl transfer reaction are 3.27 and 1.81 Å, respectively (Figure 10). The standard errors are ± 0.20 and ± 0.00 Å, respectively. The N_ϵ(MeLys)−C_γ(AdoMet)−S_δ(AdoMet) bond angle is 150 ± 8°. This ground-state bond angle is less than that of the nonmethylated reactant of the first methyl transfer reaction. The conformation favors an S_N2 methyl transfer reaction. The calculated average potential energy barrier of the second methyl transfer reaction is $\Delta E^\ddagger = 19.6 \pm 3.2$ kcal/mol. The structure of the transition state (TS−D) (Figure 11) was located by CPR (*41*) at the SCCDFTB/MM level. The normal-mode analysis shows that TS−D only has one imaginary frequency of 395 ± 21i cm^{-1}. In TS−D (Figure 11), the N_ϵ(MeLys)−C_γ(AdoMet) and C_γ(AdoMet)−S_δ(AdoMet) bond lengths are 2.37 ± 0.04 and 2.22 ± 0.04

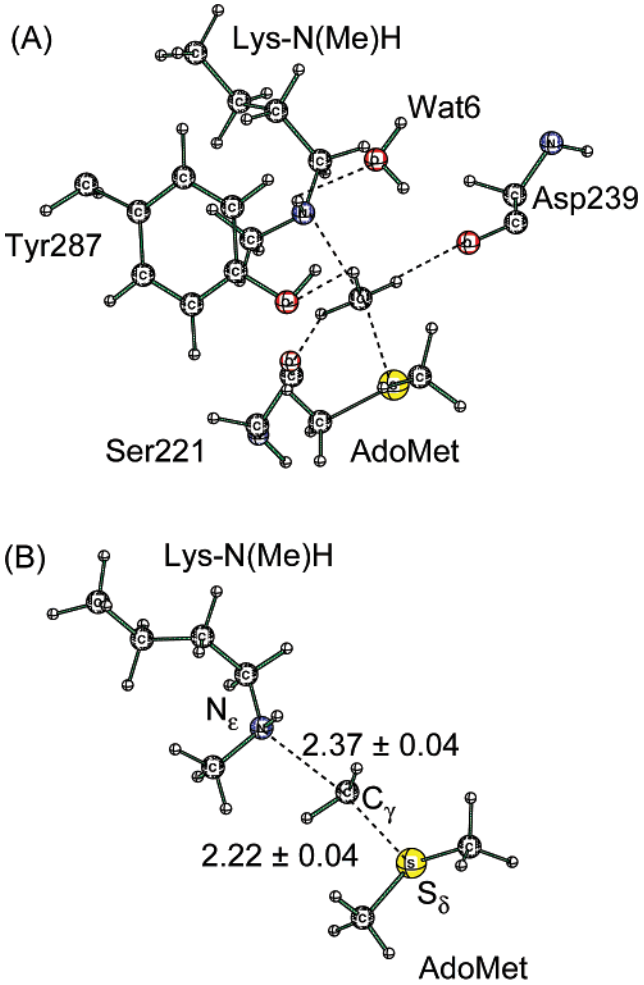

FIGURE 11: Structure of the transition state (TS−D) (A) and a close-up of the QM region (B) in the second methyl transfer reaction LSMT·AdoMet·Lys-N(Me)H → LSMT·AdoHcy·Lys-N(Me)$_2$H$^+$.

Å, respectively. The N_ϵ(MeLys)−C_γ(AdoMet)−S_δ(AdoMet) bond angle is 167 ± 6 °. Compared with TS−M (Figure 5), TS−D (Figure 11) has a longer average N_ϵ(MeLys)−C_γ(AdoMet) bond length (2.28 Å vs 2.37 Å) and a shorter average C_γ(AdoMet)−S_δ(AdoMet) bond length (2.26 Å vs 2.22 Å).

The average contributions of $\Delta(ZPE)^\ddagger = -0.12 \pm 0.39$ kcal/mol, $-T\Delta S^\ddagger = 1.48 \pm 1.28$ kcal/mol, and $\Delta E_{vib}^\ddagger = -0.46 \pm 0.42$ kcal/mol to the reaction barrier of the second methyl transfer reaction were provided by normal-mode analysis. The calculated average free energy barrier is $\Delta G^\ddagger = \Delta E^\ddagger + \Delta(ZPE)^\ddagger - T\Delta S^\ddagger + \Delta E_{vib}^\ddagger = 19.6 - 0.12 + 1.48 - 0.46 = 20.5$ kcal/mol (Figure 9), which is in reasonable agreement with the value of 22.0 kcal/mol determined from the experimental rate constant (2.5×10^{-4} s^{-1}) (*17*). The deviation in $\Delta G^\ddagger$ is ± 3.6 kcal/mol. These free energy barrier calculations are in agreement with the experimental observation that the second methyl transfer reaction is a little faster than the first one (*17*).

The second methyl transfer reaction is calculated to be exergonic overall: $\Delta G^\circ = \Delta E^\circ + \Delta(ZPE)^\circ - T\Delta S^\circ + \Delta E_{vib}^\circ = -38.2 + 3.35 + 1.24 - 0.54 = -34.2$ kcal/mol (Figure 9). The deviations in ΔG°, ΔE°, $\Delta(ZPE)^\circ$, $T\Delta S^\circ$, and ΔE_{vib}° are ±5.9 kcal/mol, ±5.9 kcal/mol, ±0.42 kcal/mol, ±1.27 kcal/mol, and ±0.43 kcal/mol, respectively. The structure of the product LSMT·AdoHcy·Lys-N(Me)$_2$H$^+$ is shown in

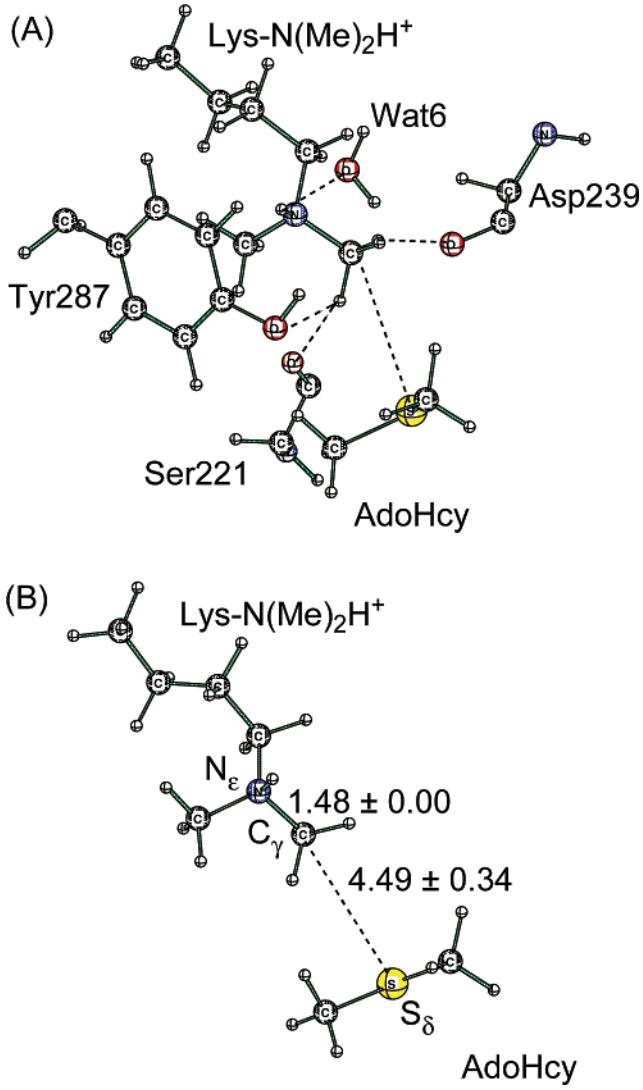

FIGURE 12: Structure of the immediate product LSMT·AdoHcy·Lys-N(Me)$_2$H$^+$ (A) and a close-up of the QM region (B) in the second methyl transfer reaction LSMT·AdoMet·Lys-N(Me)H → LSMT·AdoHcy·Lys-N(Me)$_2$H$^+$.

Figure 12. The N_ϵ(MeLys)···C_γ(AdoMet)···S_δ (AdoMet) bond angle is 151 ± 8°.

Perturbation Analysis of the Contributions from Electrostatic Interactions. The same perturbation analysis of the contribution of electrostatic interactions to the first methyl transfer reaction was applied to the second methyl transfer reaction. The perturbation analysis (*44*, *45*) for the second methyl transfer reaction (Figure 13) indicates that the favorable (and dominant) effects of Arg222 (4.02 ± 0.74 kcal/mol), Glu250 (1.51 ± 0.17 kcal/mol), Asp288 (1.37 ± 0.42 kcal/mol), Asp251 (1.10 ± 0.33 kcal/mol), and Wat6 (1.08 ± 0.47 kcal/mol) decrease the activation energy compared with that in solution or in the gas-phase model; these residues stabilize the transition state. The unfavorable contributions of Asp239 (−3.24 ± 0.62 kcal/mol), Lys291 (−2.05 ± 0.39 kcal/mol), Arg226 (−1.87 ± 0.23 kcal/mol), Glu80 (−1.79 ± 0.40 kcal/mol), Asp155 (−1.25 ± 0.25 kcal/mol), and Ser221 (−0.64 ± 0.13 kcal/mol) increase the activation energy; these residues stabilize the ground state. Stabilizing forces for the ground state and transition state differ by ∼1 kcal/mol. The contributions to transition state stabilization from Tyr287 and Tyr300 are much smaller

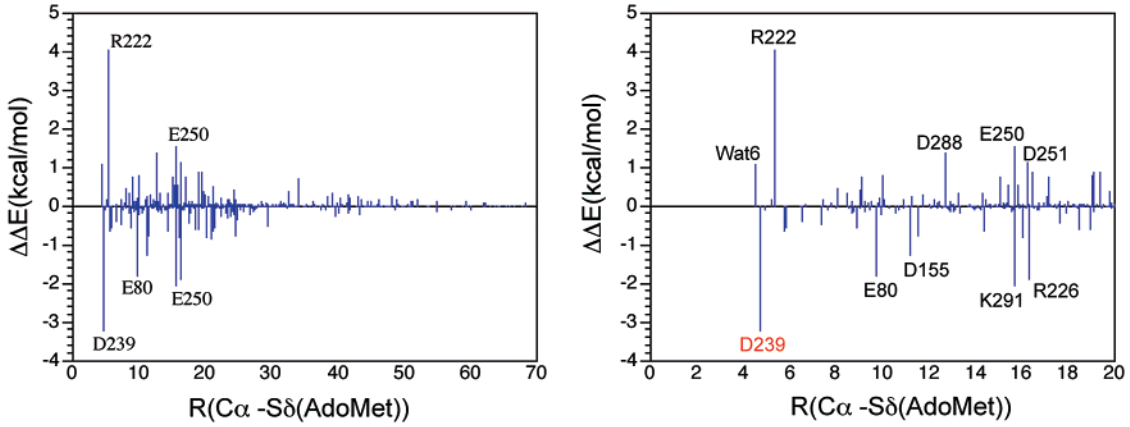

FIGURE 13: Results from perturbation analysis for the contribution from the protein residues to the activation barrier of LSMT·AdoMet·Lys-N(Me)H → LSMT·AdoHcy·Lys-N(Me)$_2$H$^+$. The positive values indicate the favorable contributions that lower the barrier; the negative values indicate the unfavorable contributions that increase the barrier.

Table 4: Distances (in Å) and the Corresponding Difference of the Key Hydrogen Bonding at the Active Site of the Transition State and the Reactant for the Second Methyl Transfer Reaction Catalyzed by LSMT

	reactant		TS		difference	
hydrogen bonds	average	deviation	average	deviation	average	deviation
HZ1(MeLys)−OH2(Wat6)	3.22	1.24	3.25	1.15	0.03	0.34
HT1(MeLys)−O(Y287)	2.93	0.37	2.94	0.37	0.01	0.02
HT2(MeLys)−OH(Y300)	3.98	1.06	3.90	1.00	−0.08	0.07
H1(Wat6)−O(D239)	3.26	1.00	3.32	1.05	0.05	0.10
HGP1(AdoMet)−O(S221)	3.05	0.78	2.99	0.71	−0.06	0.16
HGP2(AdoMet)−O(D239)	2.87	0.53	3.26	0.54	0.39	0.16
HGP3(AdoMet)−OH(Y287)	3.26	0.70	3.24	0.66	−0.02	0.08
H3T(AdoMet)−O(Y300)	1.66	0.02	1.68	0.02	0.01	0.01
OT1(AdoMet)−HH21(R222)	1.69	0.04	1.67	0.04	−0.01	0.01

(<0.5 kcal/mol). The two Tyr residues play a role in positioning the MeLys substrate and AdoMet cofactor and create the active conformers for the second methyl transfer reaction. In addition, Wat6 fluctuations are considerable going from the ground state to TS−D. Wat6 contributes favorably (1.08 ± 0.47 kcal/mol) to stabilize the transition state for the second methyl transfer reaction, whereas it hardly makes any contribution to the first methyl transfer reaction. This is due to a weaker hydrogen bond between Wat6 and O(Asp239) in the second methyl transfer reaction (Table 4).

Third Methyl Transfer Reaction

Absence of a Water Channel. The 2.5 ns MD simulations on LSMT·AdoMet·Lys-N(Me)$_2$H$^+$ do not support the formation of a water channel for proton dissociation from Lys-N(Me)$_2$H$^+$. The MD results are consistent with the observation (*17*) that the third methylation does not occur.

Free Energy Profile for the Third Methyl Transfer Reaction: Lys-N(Me)$_2$ + AdoMet → Lys-M(Me)$_3^+$ + AdoHcy. QM/MM calculations with 2D reaction coordinates were carried out on the third methyl transfer reaction. The calculated average free energy is $\Delta G^{\ddagger} = 25.9 \pm 3.2$ kcal/mol. The potential energy barrier is from single-point computations by MP2/6-31+G(d,p)//MM. The contributions of $\Delta(ZPE)^{\ddagger}$, $T\Delta S^{\ddagger}$, and $\Delta E_{vib}^{\ddagger}$ to the free energy barrier are obtained by normal-mode analysis. Because a water channel does not form to allow proton dissociation of Lys-N(Me)$_2$H$^+$, a third methylation (Scheme 1) does not occur.

The structure of the transition state (TS−T) for the third methyl transfer reaction was located by CPR (*41*) at the SCCDFTB/MM level. Normal-mode analysis shows that TS−T has a single imaginary frequency of 401 ± 16i cm^{-1}. In TS−T, the N$_\epsilon$(Me$_2$Lys)−C$_\gamma$(AdoMet) and C$_\gamma$(AdoMet)−S$_\delta$(AdoMet) bond lengths are 2.28 ± 0.04 and 2.28 ± 0.04 Å, respectively, and the N$_\epsilon$(Me$_2$Lys)−C$_\gamma$(AdoMet)−S$_\delta$(AdoMet) bond angle is 173 ± 3 °. Thus, if a proton-transfer channel was present, a third methyl transfer would occur.

CONCLUSIONS

This study establishes the catalytic mechanism and the product specificity of Rubisco LSMT. Our QM/MM calculated free energy barrier for the first and second methyl transfer reactions (Scheme 1) are 22.8 ± 3.3 and 20.5 ± 3.6 kcal/mol, respectively. These results are in excellent agreement with the free energy barriers of 23.0 and 22.0 kcal/mol calculated from the experimental rate constants (6.2 × 10^{-5} and 2.5 × 10^{-4} s^{-1}, respectively). The third methyl transfer reaction is not favored because of the lack of the possibility of proton dissociation of LSMT·AdoMet·Lys-N(Me)$_2$H$^+$ due to the absence of a water channel. Our MD simulations indicate that the formation of a water channel determines whether methylation can occur. The water channel appears in the presence of AdoMet (LSMT·Lys-NH$_3^+$·AdoMet) but is not present in the immediate product (LSMT·Lys-N(Me)H$_2^+$·AdoHcy). Stepwise AdoMet methylation of Lys-NH$_3^+$ provides the products Lys-N(Me)H$_2^+$ and Lys-N(Me)$_2$H$^+$ but not Lys-N(Me)$_3^+$. Each methyl transfer from AdoMet is preceded by proton dissociation to create the neutral amine substrate. Each deprotonation step is preceded by the formation of a water channel that passes the proton to solvent water.

ACKNOWLEDGMENT

Some of the calculations were performed at the National Center for Supercomputing Applications at the University of Illinois at Urbana−Champaign.

REFERENCES

1. Zhang, X.-D., and Bruice, T. C. (2006) The mechanism of M.HhaI DNA C5 cytosine methyltransferase enzyme: A quantum mechanics/molecular mechanics approach, *Proc. Natl. Acad. Sci. U.S.A. 103*, 6148−6153.
2. Bruice, T. C. (2006) Computational approaches: reaction trajectories, structures, and atomic motions. enzyme reactions and proficiency, *Chem. Rev. 106*, 3119−3139.
3. Zhang, X.-D., and Bruice, T. C. (2006) Reaction Mechanism of Guanidinoacetate Methyltransferase, Concerted or Stepwise, *Proc. Natl. Acad. Sci. U.S.A. 103*, 16141−16146.
4. Feng, Q., Wang, H., Ng, H. H., Erdjument-Bromage, H., Tempst, P., Struhl, K., and Zhang, Y. (2002) Methylation of H3-lysine 79 is mediated by a new family of HMTases without a SET domain, *Curr. Biol. 12*, 1052−1058.
5. Min, J., Feng, Q., Li, Z. Z., Zhang, Y., and Xu, R. M. (2003) Structure of the catalytic domain of human DOT1L: a non-SET domain nucleosomal histone methyltransferase, *Cell 112*, 711−723.
6. Jacobs, S. A., Harp, J. M., Devarakonda, S., Kim, Y., Rastinejad, F., and Khorasanizadeh, S. (2002) The active site of the SET domain is constructed on a knot, *Nat. Struct. Biol. 9*, 833−838.
7. Xiao, B., Jing, C., Wilson, J. R., and Gamblin, S. J. (2003) SET domain and histone methylation, *Curr. Opin. Struct. Biol. 13*, 699−705.
8. Xiao, B., Jing, C., Wilson, J. R., Walker, P. A., Vasisht, N., Kelly, G., Howell, S., Taylor, I. A., Blackburn, G. M., and Gamblin, S. J. (2003) Structure and catalytic mechanism of the human histone methyltransferase SET 7/9, *Nature 421*, 652−656.
9. Kwon, T., Chang, J. H., Kwak, E., Lee, C. W., Joachimiak, A., Kim, Y. C., Lee, J., and Cho, Y. (2002) Mechanism of histone lysine methyl transfer revealed by the structure of SET7/9-AdoMet, *EMBO J. 22*, 292−303.
10. Couture, J., Collazo, E., Hauk, G., and Trievel, R. C. (2006) Structural basis for the methylation site specificity of SET7/9, *Nat. Struct. Mol. Biol. 13*, 140−146.
11. Couture, J., Collazo, E., Brunzelle, J. S., and Trievel, R. C. (2005) Structural and functional analysis of SET8, a histone H4 Lys-20 methyltransferase, *Genes Dev. 19*, 1455−1465.
12. Xiao, B., Jing, C., Kelly, G., Walker, P. A., Muskett, F. W., Frenkiel, T. A., Martin, S. R., Sarma, K., Reinberg, D., Gamblin, S. J., and Wilson, J. R. (2005) Specificity and mechanism of the histone methyltransferase Pr-Set7, *Genes Dev. 19*, 1444−1454.
13. Zhang, X., Yang, Z., Khan, S. I., Horton, J. R., Tamarn, H., Selker, E. U., and Cheng, X. (2003) Structural basis for the product sepcificity of histone lysine methyltransferase, *Mol. Cell 12*, 177−185.
14. Min, J., Zhang, X., Cheng, X., Grewal, S. I., and Xu, R. M. (2002) Structure of the SET domain histone lysine methyltransferase Clr4, *Nat. Struct. Biol. 9*, 828−832.
15. Qian, C., Wang, X., Manzur, K., Farooq, S. A., Zeng, L., Wang, R., and Zhou, M. (2006) Structural insights of the specificity and catalysis of a viral histone H3 lysine 27 methyltransferase, *J. Mol. Biol. 359*, 86−96.
16. Manzur, K. L., Farooq, A., Zeng, L., Plotnikova, O., Koch, A. W., Sachchidanand, and Zhou, M. M. (2003) A dimeric viral SET domain methyltransferase specific to Lys27 of histone H3, *Nat. Struct. Biol. 10*, 187−196.
17. Trievel, R. C., Flynn, E. M., Houtz, R. L., and Hurley, J. H. (2003) Mechanism of multiple lysine methylation by the SET domain enzyme rubisco LSMT, *Nat. Struct. Biol. 10*, 545−552.
18. Couture, J., Hauk, G., Thompson, M. J., Blackburn, G. M., and Trievel, R. C. (2006) Catalytic roles for carbon-oxygen hydrogen bonding in SET domain lysine methyltransferases, *J. Biol. Chem. 281*, 19280−19287.
19. Houtz, R. L., Ponient, L., Jones, S. B., Royer, M., and Stults, J. T. (1992) Posttransitional modification in the amino-terminal of the large subunit of ribulose-1,5-bisphosphate carboxylase/oxygen from several plant species, *Plant Physiol. 98*, 1170−1174.
20. Houtz, R. L., Royer, M., and Salvucci, M. E. (1991) Partial purification and characterization of ribulose 1,5-bisphosphate carboxylase/oxygenase large subunit N-methyltransferase, *Plant Physiol. 97*, 913−920.
21. Trievel, R. C., Beach, B. M., Dirk, L. M.A., Houtz, R. L., and Hurley, J. H. (2002) Structure and catalytic mechanism of a SET domain protein methyltransferase, *Cell 111*, 91−103.
22. Rea, S., Eisenhaber, F., O'Carroll, D., Strahl, B. D., Sun, Z., Schmid, M., Opravil, S., Mechtler, K., Ponting, C. P., Allis, C. D., and Jenuwein, T. (2000) Regulation of chromatin structure by site-specific histone H3 methyltransferases, *Nature 406*, 593−599.
23. Schultz, J., Milpetz, F., Bork, P., and Ponting, C. P. (1998) SMART, a simple modular architecture research tool: Identification of signaling domains, *Proc. Natl. Acad. Sci. U.S.A. 95*, 5857−5864.
24. Cheng, X., Collins, R. E., and Zhang, X. (2005) Structural and sequence motifs of protein (histone) methylation enzymes, *Annu. Rev. Biophys. Biomol. Struct. 34*, 267−294.
25. Hu, P., and Zhang, Y. (2006) Catalytic mechanism and product specificity of the histone lysine methyltransferase SET 7/9: an *ab initio* QM/MM-FE study with multiple initial structures, *J. Am. Chem. Soc. 128*, 1272−1278.
26. Liu, Y., and Eisenberg, D. (2002) 3D domain swapping: as domains continue to swap, *Protein Sci. 11*, 1285−1299.
27. Wang, P., Royer, M., and Houtz, R. L. (1995) Affinity purification of ribulose-1,5-biphosphate carboxylate/oxygenase large subunit N-methyltransferase, *Protein Expression Purif. 6*, 528−536.
28. Jorgensen, W. L., Chandrasekhar, J., Madura, J. D., Impey, R. W., and Klein, K. L. (1983) Comparison of simple potential functions for simulating liquid water, *J. Chem. Phys. 79*, 926−935.
29. Brooks, B. R., Bruccoleri, R. E., Olafson, B. D., States, D. J., Swaminathan, S., and Karplus, M. (1983) CHARMM - a program for macromolecular energy, minimization, and dynamics calculations, *J. Comput. Chem. 4*, 187−217.
30. MacKerell, A. D., Jr., Feig, M., and Brooks, C. L., III. (2004) Extending the treatment of backbone energetics in protein force fields: limitations of gas-phase quantum mechanics in reproducing protein conformational distributions in molecular dynamics simulations, *J. Comput. Chem. 25*, 1400−1415.
31. MacKerell, A. D., Jr., Bashford, D., Bellott, M., Dunbrack, R. L., Jr., Evanseck, J.D., Field, M. J., Fischer, S., Gao, J., Guo, H., Ha, S., Joseph-McCarthy, D., Kuchnir, L., Kuczera, K., Lau, F. T. K., Mattos, C., Michnick, S., Ngo, T., Nguyen, D. T., Prodhom, B., Reiher, W. E., III, Roux, B., Schlenkrich, M., Smith, J. C., Stote, R., Straub, J., Watanabe, M., Wiorkiewicz-Kuczera, J., Yin, D., and Karplus, M. (1998) All-atom empirical potential for molecular modeling and dynamics studies of proteins, *J. Phys. Chem. B 102*, 3586−3616.
32. Brunger, A. T., Brooks, C. L., III, and Karplus, M. (1985) Active site dynamics of ribonuclease, *Proc. Natl. Acad. Sci. U.S.A. 82*, 8458−8462.
33. Brooks, C. L., and Karplus, M. (1989) Solvent effects on protein motion and protein effects on solvent motion: dynamics of the active site region of lysozyme, *J. Mol. Biol. 208*, 159−181.
34. Ryckaert, J. P., Ciccotti, G., and Berendsen, H. J. C. (1977) Numerical integration of the cartesian equations of motion of a system with constraints: molecular dynamics of n-alkanes, *J. Comput. Phys. 23*, 327−341.
35. Nicholls, A., and Honig, B. (1991) A rapid finite difference algorithm, utilizing successive over-relaxation to solve the Poisson-Boltzmann equation, *J. Comput. Chem. 12*, 435−445.
36. Klapper, I., Hagstrom, R., Fine, R., Sharp, K., and Honig, B. (1986) Focusing of electric fields in the active site of Cu-Zn superoxide dismutase: effects of ionic strength and amino-acid modification, *Proteins: Struct., Funct., Genet. 1*, 47−59.
37. Nina, M., Beglov, D., and Roux, B. (1997) Atomic radii for continuum electrostatics calculations based on molecular dynamics free energy simulations, *J. Phys. Chem. B 102*, 5239−5248.
38. Schaefer, M., Sommer, M., and Karplus, M. (1997) pH-dependence of protein stability: absolute electrostatic free energy differences between conformations, *J. Phys. Chem. B 101*, 1663−1683.
39. Cui, Q., Elstner, M., Kaxiras, E., Frauesheim, T., and Karplus, M. (2001) A QM/MM implementation of the self-consistent charge density functional tight binding (SCC-DFTB) method, *J. Phys. Chem. B 105*, 569−585.
40. Elstner, M., Porezag, D., Jungnickel, G., Elsner, J., Haugk, M., Frauenheim, Th., Suhai, S., and Seifert, G. (1998) Self-consistent-charge density-functional tight-binding method for simulation of complex materials properties, *Phys. Rev. B 58*, 7260−7268.

41. Fischer, S., and Karplus, M. (1992) Conjugate peak refinement: an algorithm for finding reaction paths and accurate transition states in systems with many degrees of freedom, *Chem. Phys. Lett. 194*, 252−261.
42. Schmidt, M. W., Baldridge, K. K., Boatz, J. A., Elbert, S. T., Gorden, M. S., Jensen, J. H., Koseki, S., Matsunage, N., Nguyen, K. A., Su, S. J., Windus, T. L., Dupuis, M., and Montgomery, J. A. (1993) General atomic and molecular electronic-structure system, *J. Comput. Chem. 14*, 1347−1363.
43. McQuarrie, D. A. (1973) *Statistical Thermodynamics*, Harper and Row, New York.
44. Zhang, X., Harrison, D. H. T., and Cui, Q. (2002) The functional specificities of methylglyoxal synthase (MGS) and triosephosphate isomerase (TIM) are not due to stereoelectronic effects: a combined QM/MM analysis, *J. Am. Chem. Soc 124*, 14871−15878.
45. Cui, Q., and Karplus, M. (2001) Triosephosphate isomerase: a theoretical comparison of alternative pathways, *J. Am. Chem. Soc 123*, 2284−2290.

BI700119P